Progress In Electromagnetics Research, Vol. 136, 79–99, 2013

AN ADVANCED UWB CHANNEL MODEL FOR BODY-CENTRIC WIRELESS NETWORKS

Raffaele Di Bari[1], Qammer H. Abbasi[1, 2, *], Akram Alomainy[1], and Yang Hao[1]

[1]School of Electronics Engineering and Computer Science, Queen Mary, University of London, London, UK

[2]Department of Electrical Engineering, University of Engineering and Technology (UET), Lahore, Pakistan

Abstract—This paper presents a novel ultra wideband (UWB) channel model in the 3–10 GHz range for body-centric wireless communications. The tests are performed in both indoor anechoic chamber environments, addressing on-body and off-body propagation scenarios. The body channel model is extracted by using a single spatial grid over all the body, and by distinguishing between LOS and NLOS condition. The large number and the uniform placement of the receiver locations attempt a representation of the body propagation links more comprehensive than previously published models. The statistical reliability of the model is investigated by applying jointly the Kolmogorov-Smirnov and the Akaike criteria. The analysis suggested that the Lognormal model fits the channel amplitude distributions with a percentage $\geq 64\%$. The on-body indoor channel amplitudes are modeled with a stochastic terms of about 4–5 dB higher than previously published models. Finally, a Negative-Binomial and Inverse Gaussian distribution are used to model the expected number of paths and interarrival time, respectively. Based on the results presented in this paper, clear recommendations are given with regards to the optimum statistical distribution of an accurate UWB body-centric radio channel modeling.

Received 29 August 2012, Accepted 5 January 2013, Scheduled 16 January 2013

* Corresponding author: Qammer Hussain Abbasi (majorqam@hotmail.com).

1. INTRODUCTION

Given the trend towards a user-centric concept in mobile communications, wireless body area networks (WBAN) have received increasing attention within the wireless personal and body area networks community [1, 2]. WBAN are attractive low cost solutions that can be used in healthcare, sports and lifestyle monitoring applications enabling constant health screening and access to patients regardless of their current location or activity. Devices like ECGs, pulse oximeter, blood pressure, insulin pumps and blood glucose can be coupled with wireless and wearable communication sensors. The UWB technology offers high data rate communication links and low power emission level, in addition to less complex system designs, which makes it a promising technology for WBAN. The human body is a demanding environment for the propagation of a wireless signal, so it is important to understand and characterize the body-centric radio channel for the design of low power and spectrum efficient wearable wireless systems. A number of Ultra Wideband (UWB) channel characterisation studies have been proposed in the past [1–40]. Alomainy et al. [3–6], performed frequency domain UWB on-body measurements and characterized on-body channels using the empirical linear path loss model. Channel characterization using transient and statistical analysis for different UWB antennas with incorporation of different postures and positions of the human body for both static and dynamic scenarios have also been discussed in [7–11]. Fort et al. [12–15], studied thoroughly the channel model for both on- and around-the-body, proposing a suitable channel model for computer based implementation.

An UWB on-body channel characterization based on path loss and time dispersion parameters has also been presented in [16–20], while the path arrival modelling is presented in [21]. The power delay profile modelling of the ultra wideband off-body propagation channel is discussed in [22–24]. In [25], UWB off-body communication channels results based on measurements result in an anechoic chamber has been published. The effect of the indoor environment on the UWB body area channel has been investigated and demonstrated in [26, 27]. A number of UWB channels valid in the 3–10 GHz range have been proposed in [28–36]. The IEEE 802.15.6 standardisation committee of wireless body area network (WBAN) technology has published a policy for channel modelling on WBAN [37], including a 3.1–10.6 GHz range model. However, the latter channel models rely on data presented in [38, 39], where the statistical model selection criterion and confidence are not discussed.

All the 3–10 GHz channels models mention beforehand are based

on a relatively limited number of receiver locations on the body, and the receiver locations are not uniformly placed around the body. Thus, the models resulting are not a comprehensive representation of the body propagation links and the statistics reliability figures are not provided. This paper addresses this issue by presenting a novel stochastic channel model based on a large number of receiver uniformly placed all over the body. Such large number of receiver locations increases significantly the statistical confidence of results and provide a comprehensive propagation model of the human body. A comparable approach has been recently presented only in [40], where a spatial grid with 69 measurement positions over all the body is used. The statistical distribution of channel parameters is estimated by using jointly the Kolmogorov-Smirnov (KS) [32] and Second Order Akaike (AICc) [41] criteria.

The additional information retrieved by this approach is compared to a standalone use of KS or AICc criterion. Results are based on both line of sight (LOS) and non line of sight (NLOS) set-up scenarios for on/off-body radio propagation scenarios. The decay of the path amplitudes, the number of paths (NoPs) and the inter-arrival times (IATs) are modelled for all scenarios. A subset of data is also extracted to model the propagation along the chest-to-waist area, where most of medical/healthcare devices are worn.

The rest of the paper is organised as follows. Section 2 describes the measurement set-up adopted in this study and details of data post processing and the statistical analysis rationale are presented. Section 3 presents the characterisation of the UWB on-body and off-body radio channel models, with a discussion of chest-to-waist model. Finally, conclusions are drawn in Section 4.

2. MEASUREMENT SETTINGS

2.1. Measurement Setup

The body-centric radio propagation channel measurements are performed in the frequency range 3–10 GHz, at a sampling rate of 1601 separate frequency points, with a sweep time of 0.8 s. The frequency sampling interval of 4.37 MHz corresponds to a maximum unambiguous excess time delay of 228.8 ns or a maximum observable distance of 68.6 m. The frequency span of 7 GHz corresponds to a maximum temporal resolution of 0.14 ns or a maximum spatial resolution of 43 mm. The time bin size is about 0.14 ns. The transmit power is set to 0 dBm and IF bandwidth is set to 3 KHz. The resulting displayed average noise level (DANL) is about -101 dBm. The two antennas were connected to a programmable vector network analyser

(Agilent N5230C PNA-X) by low loss coaxial cables to measure the transmission response (S_{21}), with cable length of 5 meter each. The PNA-X calibration tools are used to remove any frequency dependent attenuation or delay properties of these cables. A free space measurement in the anechoic chamber was performed to verify the propagation delay between the two antennas at 1 meter distance and the noise floor, observed as more than 40 dB below the peak power. This value provides sufficient dynamic range for the planned analysis. The antennas used in the measurements are the Tapered Slot Antennas (TSA) [26]. The antenna is an omnidirectional radiator with relatively constant peak gain (e.g., from 2 to 4 dB) across the whole UWB band. However, its radiation pattern and gain can be very different when placed on body [8].

In case of on-body measurements, both transmit (Tx) and receiver (Rx) antennas are placed on the body with an antenna-body separation

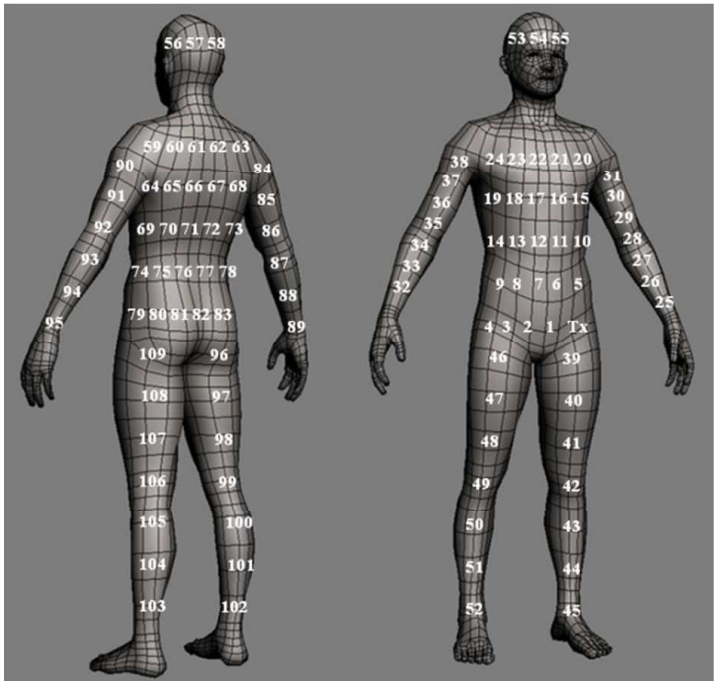

Figure 1. On-body receiver and transmit index locations for (a) NLOS and (b) LOS scenarios, considering body shadowing for back placed sensors.

of about 7 mm.

The Tx antenna was fixed at the waist and $N = 109$ different locations for Rx antenna were taken as shown in Fig. 1. Fig. 2(a) shows how the Rx antenna is oriented and placed on body. During each measurement, the subject arms were aligned along the body as shown in Fig. 2(a). In case of off-body measurements, while the Rx antenna set-up is unmodified, the Tx antenna is placed on a plastic tripod 1 m away from the body and at 1 m height from the ground as shown in Fig. 2(b). Considering the off-body case, a larger separation between the Tx and Rx antennas should not affect significantly the amplitude statistics or the number of paths, while an impact on inter-cluster arrival times, inter-time of arrivals and cluster decaying law can be expected. In both off and on-body cases, the Tx and Rx antennas are vertically aligned. The Rx location indexes within the range of 0–55 are referred as LOS, while the indexes within the range of 56–109 are referred as NLOS. A third set of data named as Generic channel is derived by combination of both LOS and NLOS measurements (e.g., receiver indexes within the range of 1–109). A set of data within the range of 1–24 is extracted from the LOS on-body measurements to model the chest-to-waist channel model. The transmitter at the chest and the receiver at the waist can be considered as a sensor and a coordinator for healthcare and medical BANs, respectively.

Measurements are first performed in the anechoic chamber to eliminate the majority of the environment multipath reflections (excepting those relative to the floor), and then repeated in the Body-Centric Wireless Sensor Lab at Queen Mary, University of London (sketched in Fig. 3) to consider the effects of the indoor environment on the body propagation channel.

2.2. Data Post-processing and Statistical Analysis

By means of later off-line processing, the measured channel transfer functions (CTFs) are transformed into the channel impulse responses (CIRs) through Inverse Fast Fourier transform (IFFT). All effects caused by movement of subject are minimized by averaging the 32 sweeps for each location. During the measurements, the room was kept empty with minimum personnel movements. To ensure that the effects of near body propagation can be separated from the multipath due to reflections from the walls, ceilings, and other surrounding objects, the human subject was seated near the centre of the room while the measuring equipment was placed at the corner. As it will be discussed in Section 3.4, the location of the objects in the room can be a source of non-randomness for the inter-arrival times.

The path components are squared to retrieve the power and a

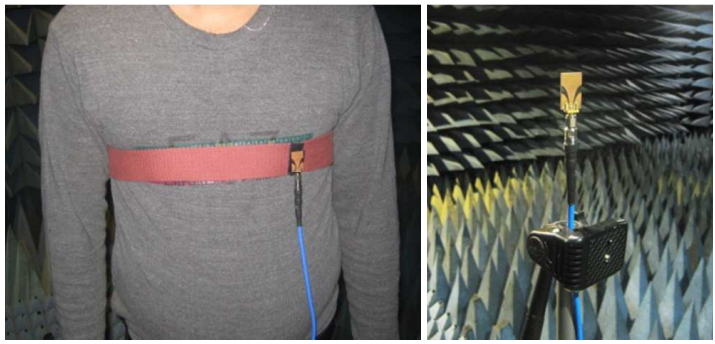

(a) (b)

Figure 2. Off-body measurement set-up for (a) the receiver antenna on index location 16 and (b) the transmit antenna.

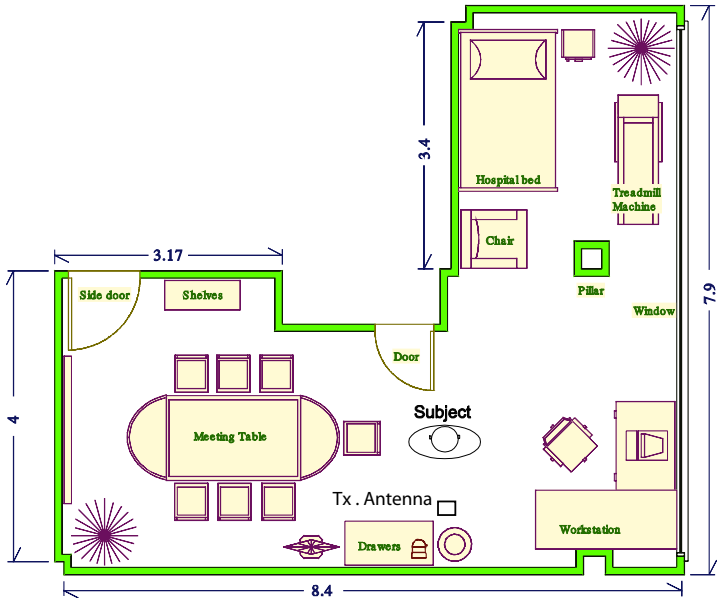

Figure 3. Dimensions and geometry of the Body-Centric Wireless Sensor Lab where the indoor radio propagation measurements are performed. The sensor lab height is 3 m.

first path detection algorithm (based on a 20 dB threshold below the peak power) is applied. Then, CIRs are aligned coherently. In case of on-body measurements, it is verified by visual inspection that the on-body, ground and other room scattering clusters are consistently

aligned.

A threshold value of 30 dB less than the amplitude of the strongest path is applied to obtain the local peaks significant for channel modelling. Finally, each CIR is normalized to its first path power to remove the path loss as described in [20]. Fig. 4(a) shows a channel impulse responses for receiver indexes in 1–109 range for on-body anechoic chamber measurements, while Fig. 4(b) shows a channel impulse responses after the alignment process. Fig. 5 shows a channel impulse CIRs at index location 76 for indoor and anechoic chamber off-body scenarios. Several parameters such as multipath components amplitudes, the inter-arrival times (Ψ), and the number of paths (Ω) are then analyzed to extract a representative stochastic model. The AICc criterion is used to evaluate the goodness of fit of the stochastic model with data as shown in [41]. However, as the AICc criterion is based on a relative distance, it is useful in selecting the best statistical distribution among a set, and it is possible that all the models from the dataset will be poor in an absolute sense [30].

A deviation from the typical theoretical distributions is expected even in cases with a strong theoretical motivation for selecting a

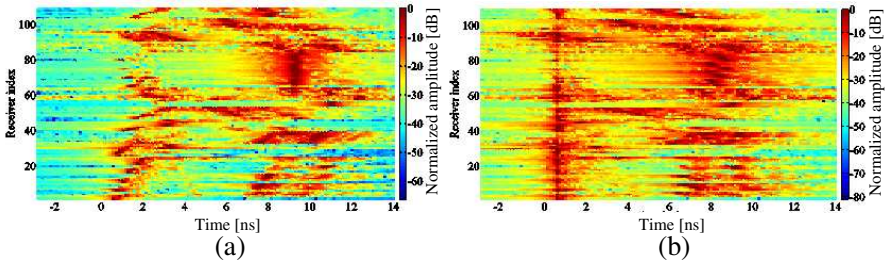

Figure 4. Sample CIRs (a) before and (b) after the alignment process for the on-body anechoic chamber channel.

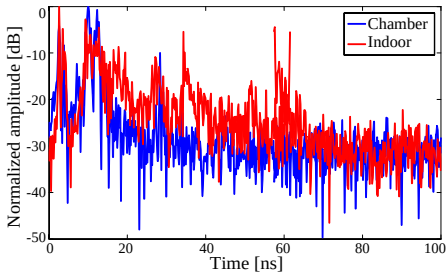

Figure 5. Sample CIRs at index location 76 for off-body scenarios.

particular distribution, as measurement errors and deviations from the theoretical developments will always occur in practice. In several cases, particularly for UWB systems, researchers used distributions which have no theoretical motivation but rather provide a reasonable empirical fit. It is worthy to mention that none of the theoretical distributions are likely to match the measured data exactly. It is entirely possible that a hypothesis test will "reject" all the proposed models for a sufficiently large data set. However, as discussed in [30] emphasis should be on determining the "best model" from a set of plausible candidates rather than "rejecting" models, because they show small deviation from the data. Thus, the rationale of using the hypothesis-test is to assess the statistical significance of the AICc selected model, rather than rejecting it. In this perspective, the KS criterion with 5% significance level testing is chosen as a complementary test. Other statistical tests commonly used in the channel modelling are the χ^2 test [32], the Kullback-Leibler (KL) information Loss [42], and the Akaike Information Criterion (AIC) [42]. A detailed discussion about these methods tradeoffs can be found in [30].

3. RESULTS

This section describes the channel model based on data from receivers uniformly placed around the body.

3.1. Kolmogorov-Smirnov and AICc Tests

The CIR is defined as:

$$h^i(t) = \sum_{l=0}^{L-1} a_l^i \exp\left(j\phi_l^i\right)\delta(t - t_l), \tag{1}$$

where i is the receiver index; a_l^i are the channel amplitudes; ϕ_l^i are the channel phases; L is the number of resolvable paths. The ϕ_l^i phases are assumed to be uniformly distributed from 0 to 2π. For a given time index l, the channel amplitudes can be represented as

$$\bar{a}_l = \left[a_l^1, a_l^2, \ldots, a_l^i, \ldots, a_l^N\right]. \tag{2}$$

The fitting is attempted by comparing the empirical cumulative distribution function (ECDF) of the vector $|\bar{a}_l|^2$ with the cumulative distribution function (CDF) of several distributions, namely Normal (N), Rayleigh (R), Weibull (W), Nakagami (NK) and Lognormal (L). The distribution parameters are estimated with Maximum-Likelihood (ML) criterion. The KS criterion and AICc tests are performed after

extracting the power $|\bar{a}_l|^2$ of every time index. Whenever the $|\bar{a}_l|^2$ data set is not compatible with the proposed CDF the hypothesis is rejected and the KS test fails.

In case of the AICc test, the number of times a proposed CDF has the best fit is estimated. Table 1 presents the KS criterion and AICc passing rate for all channels under test. According to the KS criterion, the datasets $|\bar{a}_l|^2$ seems compatible most of times with both Weibull and Lognormal distributions, with a passing rate $\geq 91\%$. On the other hand, the AICc results show a clear tendency of the lognormal CDF to be the best fitting model for all test conditions. Lognormal fitting is particularly effective in on-body anechoic chamber and off-body indoor scenarios. However, the Weibull distribution has a significant passing rate percentage for all test cases as well. For instance, for the on-body LOS indoor scenario, the Weibull model has a passing rate of 26.16%, while the lognormal model is about 63.8% However, if the data analysis is time-windowed for a 0–3 ns interval (e.g., not considering the indoor reflections), the AICc lognormal passing rate according is $\geq$ 90%. This trend has been verified with all other indoor case scenarios. Thus, the lognormal distribution can be associated with the components diffracting around the body, while the Weibull distribution better describes the ground and walls reflection components.

Table 1. KS criterion and AICc tests passing rate (%) for $|\bar{a}_l|^2$.

$\|\bar{a}_l\|^2$			KS criterion					AICc				
Scenarios			*N*	*R*	*W*	*NK*	*L*	*N*	*R*	*W*	*NK*	*L*
On-body	Chamber	LOS	1.1	2.2	100	31.4	100	0	0	10.1	0	89.9
		NLOS	0	1.1	98.8	20.0	100	0	0	18.8	0	81.2
		Generic	0	0	91.1	23.7	100	0	0	15.84	0	84.1
	Indoor	LOS	1.8	9.6	100	58.5	100	0.3	5.6	26.16	4.01	63.8
		NLOS	0	2.7	97.2	27.7	99.1	0	0.3	6.02	0.3	93.37
		Generic	0	0.5	95.01	15.3	99.4	0	0.29	10.4	0	89.3
Off-body	Chamber	LOS	2.7	25.6	100	52.7	100	0	9.4	13.5	2.7	74.3
		NLOS	0	0	100	16	100	0	0	12	2	86
		Generic	0	0	92.15	7.89	100	0	0	9.2	3.9	86.84
	Indoor	LOS	1.28	17.1	98.28	47.63	100	0	9.01	10.3	0.43	80.25
		NLOS	0	0	97.0	14.5	99.2	0	0	6.54	0	93.45
		Generic	0	0	94.9	9.11	99.6	0	0	12.56	0	87.4

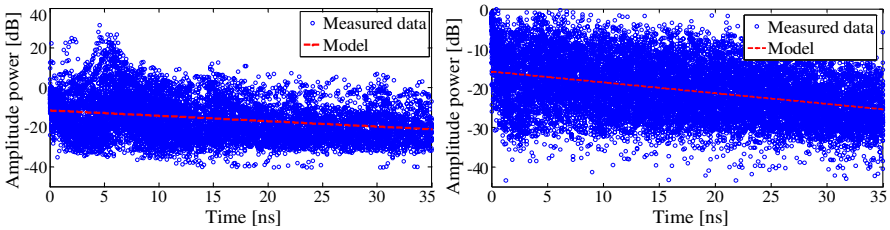

Figure 6. m_0 and Γ on the amplitude power $10\log_{10}|\bar{a}_l|^2$ for (a) on-body and (b) off-body indoor NLOS scenario.

3.2. Channel Amplitudes

Although it seems reasonable to expect a dependency of the CDF models with the excess time delay, most of researchers used a single cluster distribution and a standard variation value to model all the bins in order to provide a compact model [20, 30, 37, 43]. The results presented in Table 1 provide a confidence indication about choosing the lognormal CDF as single distribution model for each test scenario. The decay of the path amplitudes is modelled with an exponential function and with a constant factor m_0 [17]:

$$10\log_{10}\left(|\bar{a}_l|^2\right) = m_0 + 10\log_{10}\left(\exp\left(\frac{t_l}{\Gamma}\right)\right) + S \tag{3}$$

where $l = 0, 1, \ldots, L$, and S is a stochastic term. The term S is modelled by a Lognormal distribution with zero-mean and standard deviation σ_S, consistently with several previous wideband and UWB small-scale fading studies [44, 45] and the 802.15.6 standardization WBAN channel model [37]. Fig. 6 shows the amplitudes power $10\log_{10}|\bar{a}_l|^2$ for both on-body (a) and off-body (b) sample cases for an indoor NLOS scenario. A regression curve obtained through least squares fitting is also plotted.

In Table 2, the values of m_0, Γ are derived from the regression curves (indicated with M) and compared with literature values (indicated with LV). The values of σ_S are derived by the Lognormal fitting among differences between measured data and the regression as shown in Fig. 7. For simplicity, the dependence of σ_S with excess time delay is not considered. As reference, Γ for the on-body LOS in anechoic chamber is 13.4 ns and it gives a close agreement with the same test scenario results presented in [20] (e.g., 8.9 ns). The 16.5–49.3 ns Γ range estimated for the on-body indoor compares with the 59.7 ns presented in [37], while Γ for the off-body LOS indoor 11.3 ns approaches the 14.6 ns presented in [32] for a similar test case scenario.

Table 2. Measured values for PDP parameters.

Scenario			Taps amplitude fitting parameters $\lvert\bar{a}_l\rvert^2$				
			m_0 [dB]	Γ [ns]		σ_S [dB]	
			M	*M*	*LV*	*M*	*LV*
On-body	Chamber	LOS	−13.9	13.4	8.9 [20]	11.6	2.9 [37]
		NLOS	−7.5	11.9		11.7	
		Generic	−10.7	14.2		11.9	
	Indoor	LOS	−19.8	49.3	59.7 [37]	10.1	5.0 [37] 4.97 [38]
		NLOS	−13.3	16.5		9.9	
		Generic	−16.4	24.6		10.1	
Off-body	Chamber	LOS	−23.0	1.86		8.7	
		NLOS	−16.8	4.95		9.03	
		Generic	−21.0	5.12		10.1	
	Indoor	LOS	−26.2	11.3	14.6 [32]	7.1	7.3 [37]
		NLOS	−15.3	16.5		7.2	
		Generic	−22.2	35.6		8.7	

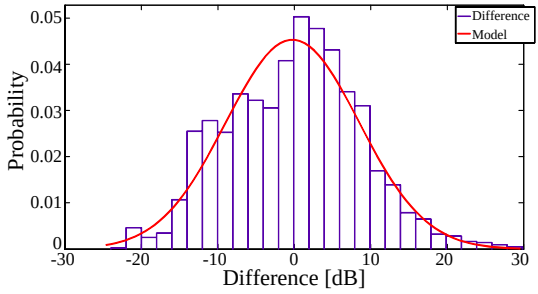

Figure 7. σ_S on the on the power amplitude $|\bar{a}_l|^2$ for on- body indoor LOS.

The range σ_S for on-body anechoic chamber is 11.6–11.9 dB and it differs significantly from the 2.9 dB shown in [37]; however, the reflections from the ground are not included in the latter. For the on-body indoor scenario, the estimated range of 9.8–10.1 dB again diverges significantly from the 5.02 dB presented in [37] and the 4.97 dB in [38]. However, as in [37, 38] the volunteer body lies on a bed, the ground reflections are likely to fall within the body signal cluster, contributing to lowering σ_S. As it will be shown later in the paper, the threshold

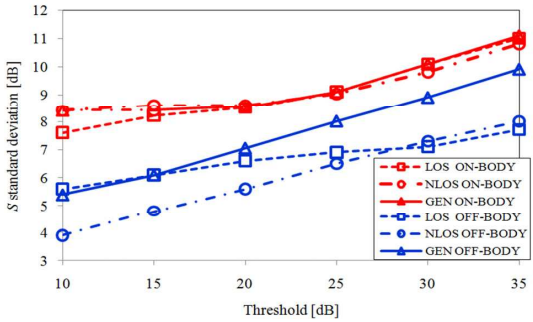

Figure 8. σ_S for off and on-body indoor scenario against threshold values.

selected also have a significant impact.

The room dimensions are expected to influence the maximum excess time delay, while the materials and the number of objects should affects the number and the power of the scattered paths. By comparing the chamber and indoor results in Table 2, these parameter mainly impact on the fitting curve slope Γ (rather than σ_S).

The range of σ_S for off-body indoor case varies from 7.1–8.7 dB and it is found to be similar to the 7.03–7.3 dB presented in [37].

As σ_S does not change significantly from the Generic channel to NLOS or LOS, it is envisaged that σ_S is weakly correlated to the number of receivers. On the other hand, σ_S. appears to be strongly correlated to the power threshold. Fig. 8 shows σ_S for off- and on-body indoor scenario for different threshold values. Considering the on-body scenario, if a lower threshold level is employed (e.g., 10–15 dB), only the most significant multipath components are taken into account. Thus, the model tends to be more "deterministic" as σ_S falls within the 7.5–8.5 dB range. The σ_S values relative to the off-body scenario reduce almost linearly with the threshold values, and for the same threshold level, the values falls within 4–5.5 dB range. Thus, it can be concluded that considering a 30 dB threshold, the on-body indoor channel model shows a stochastic terms about 4–5 dB higher than previous models, while the off-body indoor channel model is still within the range of previous published results.

3.3. Number of Paths

The Ω CDF is estimated by comparing the Poisson (P) and negative-binomial (NB) distributions. In this case, the KS criterion has not been performed as it is valid only for continuous distributions. Fig. 9 shows

the NB superior fitting for the sample off-body LOS indoor scenario if compared with the Poisson distribution employed in [30, 37]. The distribution parameters are estimated with ML criterion and reported in Table 3. The parameters r and p are commonly referred as the number of successes in the negative binomial experiment and the success probability in each trial, respectively.

The mean number of paths (L) for on-body indoor environment is within the range of 146–179 and diverges from the value of 38 shown in [38]. This discrepancy depends again on the power threshold

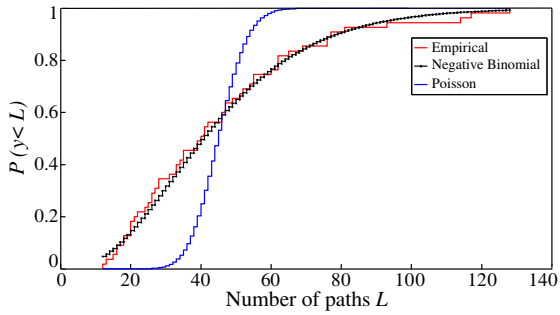

Figure 9. CDF for the number of paths for off-body LOS indoor set-up.

Table 3. Derived values for the PDP parameters.

Scenario			Number of Paths (Ω)			Inter-time of Arrivals (ψ)		
			CDF	L (mean)	Parameters: r, p	CDF	μ_τ	λ_τ
On-body	Chamber	LOS	NB	56	10.6, 0.15	INVG	0.19	0.7
		NLOS		68	7.27, 0.17		0.17	1.3
		Generic		64	11.4, 0.15		0.18	0.87
	Indoor	LOS		146	1.6, 0.01		0.26	0.43
		NLOS		179	3.37, 0.02		0.23	0.5
		Generic		164	2.14, 0.12		0.24	0.46
Off-body	Chamber	LOS		37	6.55, 0.15		0.2	0.71
		NLOS		72	31.9, 0.3		0.15	4.05
		Generic		51	6.07, 0.1		0.17	1.12
	Indoor	LOS		132	8.9, 0.06		0.24	0.5
		NLOS		237	5.428, 0.1		0.16	1.84
		Generic		196	5.4, 0.02		0.19	0.77

selected: in fact, L is within the range of 41–66 considering a 20 dB threshold as [32]. The range of L for off-body indoor scenario is 132–196 and significantly diverges from the value of 400 presented in [39]. This depends on the size of the reference test room significantly larger of the one used for this research.

3.4. Inter-time of Arrivals.

The delay time of each ray from the corresponding peak in the power delay profile is identified, and the differences between the arrival times of two successive paths are calculated in order to obtain Ψ [34].

According to the model presented in [37], the intervals between individual counts (e.g., Ψ) should follow an exponential probability density function with a fixed path arrival rate. As the Poisson and exponential distributions are related, if Ψ follows the exponential distribution, the number of counts (e.g., the arrival times) follows the Poisson distribution. However, in several cases, measurement shows that the single exponential process is insufficient to model Ψ. Thus, a mixture of two exponential processes (EXM) has been proposed to model Ψ in [32, 46, 47]. In [13], the authors model the path inter-arrival times by using the Weibull distribution as a result of the non-randomness of the local structures in an indoor environment. However, this model has been applied only for rays within the first cluster of the impulse response, which is not the general case. Finally [48] indicates that Inverse Gaussian (INVG) distribution provides the best fitting for chest-to-waist scenario. Thus, the statistical distributions selected to fit Ψ are the Exponential, Weibull, Exponential Mixture (EXM), and Inverse Gaussian [48].

Figure 10 shows the empirical CDF and fitting models for Ψ Although it is envisaged from visual inspection that the EXM has better fitting with the empirical model, the AICc test indicates the INVG as the best candidate model for all scenarios case. This because the AICc penalizes the EXM as having 3 parameters, while the INVG has only 2. The mean (μ_τ) and the scaling factor (λ_τ) parameters are estimated with the ML criterion. As reference, the values for on-body LOS anechoic chamber are $\mu_\tau = 0.15 - 0.17$ and $\lambda_\tau = 0.7 - 1.3$ and they compare with $\mu_\tau = 0.33$ and $\lambda_\tau = 0.85$ presented in [48].

Although the INVG is the best model according to the AICc criterion, the KS criterion test rejects all the proposed distributions for all test case scenarios, suggesting a statistically significant deviation from the measured data. Thus, more complex models such as the Modified-Poisson [21] might be employed in predicting the path arrival times satisfying the KS criterion as well.

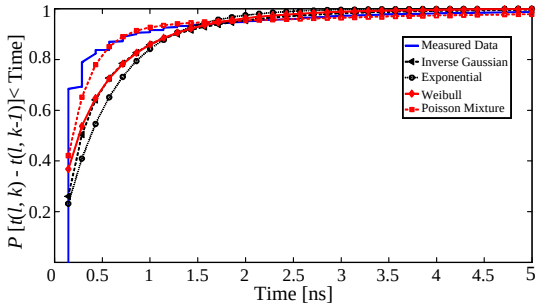

Figure 10. Empirical CDF and fitting models of Ψ for off-body LOS indoor.

Table 4. Derived values for the chest-to-waist PDP parameters.

Scenario	Taps amplitude fitting parameters $\lvert\bar{a}_l\rvert^2$			Number of Paths (Ω)			Inter-time of Arrivals (ψ)		
	m_0 [dB]	Γ [ns]	σ_S [dB]	CDF	L (mean)	Parameters: r, p	CDF	μ_τ	λ_τ
Chamber	−1398	12.27	11.4	NB	58	8.4, 0.12	INVG	0.2	0.63
Indoor	−17.28	39.6	10.4	NB	168	2.8, 0.04	INVG	0.22	0.54

3.5. Chest-to-waist Model

The data are retrieved by considering the receivers indexes in the range 1–24 as shown in Fig. 1. While the KS criterion shows a passing rate for the Lognormal distribution of about 100%, the AICc criterion yield a 59.3% and 64.3% for the anechoic chamber and indoor, respectively. With the same procedure described above, a single distribution and a standard deviation value is selected to model all the bins, and an exponential fitting model is derived. As σ_S does not differs significantly from LOS on-body channel in Table 4, a weak correlation between the number of receivers and σ_S is envisaged again. Similarly, m_0, Γ, Ω and Ψ ranges are within the data ranges relative to the whole body presented before.

4. CONCLUSIONS

An advanced UWB body-centric radio propagation channel has been derived by an extensive measurement campaign. Measurements were performed both in an anechoic chamber and in the indoor environment, and the channel responses were captured using ultra wideband

frequency domain measurement set-up. The results show the superior fitting of lognormal distribution for channel modelling when more than 100 receivers are heterogeneously placed on body to model the on- and off-body channel. The benefits of this approach consist of having a propagation model more comprehensive compared to those presented in the open literature. According to KS criterion, the channel amplitudes are compatible mostly with both Weibull and Lognormal distributions, with a passing rate $\geq 91\%$. However, the AICc suggests a percentage from 63.8% to 93.45% depending on the scenario investigated. In the case of the chest-to-waist channel model, the KS criterion shows that passing rate for the lognormal distribution is more than 95%, the AICc shows a 59.3% and 64.3% for the anechoic chamber and indoor, respectively.

The standard variation of the on-body indoor channel models is about 4–5 dB higher than previous models with a 30 dB detection threshold. It is suggested that higher values mostly depend on the power threshold and test conditions, and secondarily on the large number of receivers. Unlike previously published results, the number of paths is modelled with a Negative-Binomial distribution. Considering the inter-arrival paths, although the Inverse Gaussian resulted to be the best model according to AICc, the KS criterion shows that all models have some significant statistical deviation from the data. This outcome proved the effectiveness of combined KS and AICc criteria methodology.

Future research in this area could focus on measuring and analyzing different ranging scenarios and environments. It is also envisaged that a more accurate channel model can be derived using multiple clusters and associating to each cluster its own statistical distribution; the trade off would a more complex channel with increased number of parameters.

REFERENCES

1. Batra, A., J. Balakrishnan, G. R. Aiello, J. R. Foerster, and A. Dabak, "Design of a multiband OFDM system for realistic UWB channel environments," *IEEE Trans. on Microwave Theory and Techniques*, Vol. 52, No. 9, 2123–2138, Sept. 2004.
2. Abbasi, Q. H., A. Sani, A. Alomainy, and Y. Hao, "On-body radio channel characterization and system-level modeling for multiband OFDM ultra-wideband body-centric wireless network," *IEEE Trans. on Microwave Theory and Techniques*, Vol. 58, No. 12, 3485–3492, Dec. 2010.
3. Abbasi, Q. H., A. Sani, A. Alomainy, and Y. Hao, "Numeri-

cal characterisation and modelling of subject-specific ultra wideband body-centric radio channels and systems for healthcare applications," *IEEE Transaction on Information and Technology in Biomedicine*, Vol. 16, No. 2, 221–227, Mar. 2012.

4. Alomainy, A., Y. Hao, C. G. Parini, and P. S. Hall, "On-body propagation channel characterisation for UWB wireless body-centric networks," *IEEE Antennas and Propagation Society International Symposium*, Vol. 1B, 694–697, 2005.
5. Alomainy, A., Y. Hao, X. Hu, C. G. Parini, and P. S. Hall, "UWB on-body radio propagation and system modeling for wireless body-centric networks," *IEE Communications Proc.*, Vol. 153, No. 1, 107–114, 2006.
6. Abbasi, Q. H., M. M. Khan, S. Liaqat, A. Alomainy, and Y. Hao, "Experimental investigation of ultra wideband diversity techniques for on-body radio communications," *Progress In Electromagnetics Research C*, Vol. 34, 165–181, 2013.
7. Abbasi, Q. H., A. Sani, A. Alomainy, and Y. Hao, "Arm movements effect on ultra wideband on-body propagation channels and radio systems," *Loughborough Antennas and Prop. Conf.*, 261–264, Loughborough, UK, Nov. 2009.
8. Alomainy, A., A. Sani, J. Santas, A. Rahman, and Y. Hao, "Transient characteristics of wearable antennas and radio propagation channels for ultra wideband body-centric wireless communications," *IEEE Trans. on Antennas Prop.*, Vol. 57, No. 4, 875–884, Apr. 2009.
9. Alomainy, A., Y. Hao, and C. G. Parini, "Transient and small-scale analysis of ultra wideband on-body radio channel," *North American Radio Science Meeting URSI*, Ottawa, Canada, 2007.
10. Sani, A., A. Alomainy, and Y. Hao, "Time domain characterization of ultra wideband wearable antennas and radio propagation for body-centric wireless networks in healthcare applications," *Proc. of the 5th Intern. Workshop on Wearable and Implantable Body Sensor*, Hong Kong, China, 2008.
11. Khan, M. M., Q. H. Abbasi, S. Liaqat, and A. Alomainy, "Comparison of two measurement techniques for UWB off-body radio channel characterisation," *Progress In Electromagnetics Research M*, Vol. 27, 179–189, 2012.
12. Fort, A., C. Desset, P. De Doncker, P. Wambacq, and L. Van Biesen, "An ultra-wideband body area propagation channel model — From statistics to implementation," *IEEE Trans. on Microwave Theory and Techniques*, Vol. 54, No. 4, 1820–1826, Apr. 2006.

13. Fort, A., J. Ryckaert, C. Desset, P. De Doncker, P. Wambacq, and L. Van Biesen, "Ultra-wideband channel model for communication around the human body," *IEEE J. on Selected Areas in Comm.*, Vol. 24, No. 4, 927–932, Apr. 2006.
14. Fort, A., C. Desset, J. Ryckaert, P. D. Doncker, L. V. Biesen, and S. Donnay, "Ultra wideband body area channel model," *Intern. Conf. on Comm.*, Vol. 4, 2840–2844, Seoul, South Korea, May 2005.
15. Molisch, A. F., K. Balakrishnan, D. Cassioli, C. Chong, S. Emami, A. Fort, J. Karedal, J. Kunisch, H. Schantz, and K. Siwiak, "A comprehensive model for ultra wideband propagation channels," *IEEE Global Telecomm. Conf.*, St. Louis, MO, Dec. 2005.
16. Kovacs, I., G. Pedersen, P. Eggers, and K. Olesen, "Ultra wideband radio propagation in body area network scenarios," *IEEE Int. Symp. on Spread Spectrum Techniques and Applications Techniques and Applications*, 102–106, Sydney, Australia, Sept. 2004.
17. Zasowski, T., F. Althaus, M. Stager, A. Wittneben, and G. Troster, "UWB for non invasive wireless body area networks: Channel measurements and results," *IEEE Conf. on Ultra Wideband Systems and Technologies*, 285–289, Nov. 2003.
18. Abbasi, Q. H., M. M. Khan, A. Alomainy, and Y. Hao, "Sectorised radio channel characterisation for ultra wideband body-centric wireless communications," *Proc. of the 5th European Conf. on Antennas and Prop.*, 191–195, Apr. 2011.
19. Khan, M. M., Q. H. Abbasi, A. Alomainy, and Y. Hao, "Study of line of sight (LOS) and none line of sight (NLOS) ultra wideband off-body radio propagation for body centric wireless communications in indoor," *Proc. of the 5th European Conf. on Antennas and Prop.*, 110–114, Apr. 2011.
20. Takizawa, K., T. Aoyagi, J. Takada, N. Katayama, K. Yekeh, Y. Takehiko, and K. R. Kohno, "Channel models for wireless body area networks," *IEEE 30th Annual Intern. Conf. of Engineering in Medicine and Biology Society,* 1549–1552, Vancouver, Canada, 2008.
21. Goulianos, A. A. and S. Stavrou, "UWB path arrival times in body area networks," *IEEE Antennas and Wireless Prop. Letters*, Vol. 6, 223–226, 2007.
22. Goulianos, A. A., T. Brown, and S. Stavrou, "Power delay profile modelling of the ultra wideband off-body propagation channel," *IET Microwave Antennas Prop.*, Vol. 4, No. 1, 62–71, 2010.
23. Catherwood, P. A. and W. G. Scanlon, "Link characteristics for

an off-body UWB transmitter in a hospital environment," *Loughborough Antennas and Prop. Conf.*, 569–572, Loughborough, UK, Nov. 2009.

24. Xia, L., S. Redfield, and P. Chiang, "Experimental characterization of a UWB channel for body area networks," *EURASIP Journal on Wireless Communications and Networking*, Vol. 2011, 2011.
25. Goulianos, A. A., T. W. Brown, and S. Stavrou, "Ultra-wideband measurement and results for sparse off-body communication channels," *Loughborough Antennas and Prop. Conf.*, 213–216, Loughborough, UK, 2008.
26. Rahman, A., A. Alomainy, and Y. Hao, "Compact body-worn coplanar waveguide fed antenna for UWB body-centric wireless communications," *2nd European Conf. on Antennas and Prop.*, 1–4, Nov. 2007.
27. Alomainy, A., Y. Hao, C. G. Parini, and P. S. Hall, "Comparison between two different antennas for UWB on body propagation measurements," *IEEE Antennas and Wireless Prop. Letter*, 31–34, 2005.
28. Niemela, V., A. Rabbachin, A. Taparugssanagorn, M. Hamalainen, and J. Iinatti, "A comparison of UWB WBAN receivers in different measured hospital environments," *3rd International Symposium on Applied Sciences in Biomedical and Communication Technologies*, 1–5, Nov. 7–10, 2010.
29. Hamalainen, M., A. Taparugssanagorn, R. Tesi, and J. Iinatti, "Wireless medical communications using UWB," *IEEE International Conference on Ultra-Wideband*, 485–489, Sept. 2009.
30. Fort, A., "Body area communications: Channel characterization and ultra-wideband system-level approach for low power," Ph.D. Thesis, Nov. 2007.
31. Fort, A., J. Ryckaert, C. Desset, P. De Doncker, P. Wambacq, and L. Van Biesen, "Ultra wide-band channel model for communication around human body," *IEEE J. Sel. Areas Commun.*, Vol. 24, No. 4, 927–933, Apr. 2006.
32. Molisch, A. F., K. Balakrishnan, D. Cassioli, C. Chong, S. Emami, A. Fort, J. Karedal, J. Kunisch, H. Schantz, K. Siwiak, and U. Schuster, IEEE 802.15.4a Channel Model — Final Report, Tech. Rep. Document IEEE 802.15-04-0662-02-004a, 2005.
33. Molisch, A. F., D. Cassioli, C. Chong, S. Emami, A. Fort, B. Kannan, J. Karedal, J. Kunisch, H. G. Schantz, K. Siwiak, and M. Z. Win, "A comprehensive standardized model for ultrawideband propagation channels," *IEEE Trans. on Antennas*

Prop., Vol. 54, No. 11, 3151–3166, Nov. 2006.

34. Wang, Q., T. Tayamachi, I. Kimura, and J. Wang, "An on-body channel model for UWB body area," *IEEE Trans. on Antennas Prop.*, Vol. 57, No. 4, 163–170, Apr. 2009
35. Di Bari, R., Q. Hussain Abbasi, A. Alomainy, and Y. Hao, "Statistical analysis of small-scale channel parameters for ultra wideband radio channels in body-centric wireless networks," *IEEE Intern. Symp. on Antennas and Prop.*, 412–415, Spokane, USA, Jul. 2011.
36. Hamalainen, M., A. Taparugssanagorn, and J. Iinatti, "On the WBAN radio channel modelling for medical applications," *Proceedings of the 5th European Conference on Antennas and Prop.*, 2967–2971, Apr. 2011.
37. Yazdandoost, K. Y. and K. Sayrafian-Pour, "Channel model for body area network (BAN)," Tech. Rep. IEEE P802.15-08-0780-12-0006, Nov. 2010.
38. Aoyagi, T., J. Takada, K. Takizawa, N. Katayama, T. Kobayashi, K. Y. Yazdandoost, H. Li, and R. Kohno, "Channel model for wearable and implantable WBANs," Tec. Rep. IEEE 802.15-08-0416-04-0006, Nov. 2008.
39. Sawada, H., T. Aoyagi, J. Takada, K. Y. Yazdandoost, and R. Kohno, "Channel model between body surface and wireless access point for UWB band," Tec. Rep. IEEE 802.15-08-0576-00-0006, Aug. 2008.
40. Kobayashi, T., "Measurements and modeling of UWB radio propagation for wireless body area networks," *International Symposium on Applied Sciences in Biomedical and Communication Technologies*, Barcelona, Spain, Oct. 2011.
41. Sani, A., A. Alomainy, G. Palikaras, Y. Nechayev, Y. Hao, C. Parini, and P. S. Hall, "Experimental characterization of UWB on-body radio channel in indoor environment considering different antennas," *IEEE Trans. on Antennas Prop.*, Vol. 58, No. 1, 238–241, Jan. 2010.
42. Akaike, H., "Information theory as an extension of the maximum likelihood principle," *Proceedings from Second International Symposium on Information Theory*, 267–281, 1973.
43. Fort, A., J. Ryckaert, C. Desset, P. De Doncker, P. Wambacq, and L. Van Biesen, "Ultra wide-band channel model for communication around human body," *IEEE J. Sel. Areas Commun.*, Vol. 24, No. 4, 927–933, Apr. 2006.
44. Suzuki, H., "A statistical model for urban radio propagation,"

IEEE Trans. on Comm., Vol. 25, 673–680, Jul. 1977.

45. Hashemi, H., "Impulse response modeling of indoor radio propagation channels," *IEEE J. on Selected Areas in Comm.*, Vol. 11, No. 7, 967–977, Sept. 1993.
46. Molisch, A. F., "Ultrawideband propagation channels-theory, measurements, and modeling," *IEEE Trans. Veh. Technol.*, Vol. 54, No. 5, 1528–1544, Sept. 2005.
47. Chong, C. C. and S. Yong, "A generic statistical-based UWB channel model for high-rise apartments," *IEEE Trans. on Antennas Prop.*, Vol. 53, No. 8, 2389–2399, Aug. 2005.
48. Wang, Q. and J. Wang, "Performance of on-body chest-to-waist UWB communication link," *IEEE Microwave and Wireless Components Letters*, Vol. 19, No. 2, Feb. 2009.